Metal-tetraporphyrazine intercalated Mxene as electrocatalyst for oxygen reduction and evolution

UNIVERSITY OF THE
WITWATERSRAND,
JOHANNESBURG

Honors 1st Semester Research Project

Submitted by

Pheletso Marumoloe (2168828)

Supervised by

Prof. Kenneth I. Ozoemena

Co-Supervised by

Dr. Thapelo P. Mofokeng

Refiloe P. Modise

Table of contents.

Introduction…….(3)

Experimental procedure……(6)

Results and Discussion……..(9)

Conclusion……...(15)

References……(16)

Introduction

Fossil fuels have been the primary source of energy for the past several decades. The process of producing energy from fossil fuels emits harmful chemicals into the atmosphere. [1] These emissions contribute to climate change and give rise to environmental pollution through the release of various pollutants. Consequently, this situation presents significant health risks to human beings, as it leads to adverse health consequences.. [2] Thus, this leads to a demand for alternative sources of energy, that are environmentally friendly, sustainable, and affordable as well as, energy conversion and storage technologies to meet the growing demands of energy owing to the growing global population and the fourth industrial revolution.

Energy storage refers to the process of capturing and storing energy for later use. Its importance has increased significantly in recent years, necessitating a closer examination. To illustrate this, we can consider the power grid as an example. Power operators face the ongoing challenge of maintaining a stable equilibrium between energy supply and demand, particularly during periods of peak demand.. [3] Traditionally, power grids do not store electricity due to their significant cost implications. Therefore, power utilities must use more fossil fuel facilities to meet the demand. [3 This approach is not optimal because power plants operate at full capacity power to be effective, so burning more fossil fuels cannot be sustained and more power plants are being used, resulting in increased overall pollution as the other power plants try to meet the base-load demand for the utility. [3]

Currently, there is a growing exploration and implementation of alternative energy sources, such as wind and solar power. These sources have gained significant attention due to their environmentally friendly nature, sustainability, renewability, and cost-effectiveness.. However, they exhibit disadvantages, for instance, the sun does not shine at night and wind conditions are not ideal in many locations. [3] Subsequently, the power grid’s demand for frequency regulation is increased by these disadvantages. [3] Ultimately, the grid becomes unstable because it must compensate for the insufficient energy being stored when there is little or no sunshine as well as less wind availability. [3] Therefore, the have been mitigation strategies implemented to address or balance the supply and

demands of energy such as briefly turning on and off specific areas of the grid, also known as load reduction. [3] This is why there is a growing interest in energy storage technology and its corresponding devices such as batteries. [3]

The inherent capability of energy storage devices to provide a backup power in the event of grid failure is highly desirable for both commercial and residential consumers. This desirable feature enables utilities to store surplus energy generated by their facilities during periods of low demand and subsequently release it when demand rises

. [3]

Energy conversion and storage technologies such as fuel cells (FCs), electrolyzers and metal-air batteries have received a lot of attention in recent years. In these devices, redox processes are used to (i) convert chemical energy to electrical energy in FCs, (ii) produce fuel like hydrogen (H_2) and oxygen (O_2) in electrolyzers which in turn can be used in FCs as the chemicals and (iii) storage of chemical energy from metals like zinc (Zn) coupled with oxygen (O_2) from air, like in a zinc-air battery. [4,5,6]In a rechargeable zinc-air battery (RZAB), electrical energy is stored from the redox processes that take place on the zinc anode and air cathode compartments as shown by Figure 1.

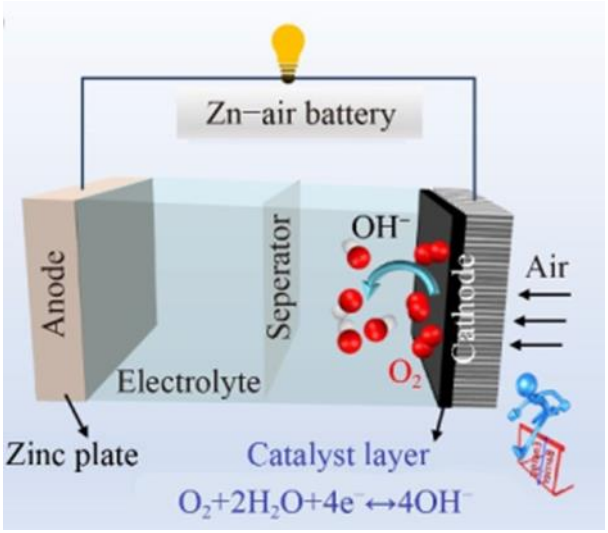

Figure 1: Representation of a rechargeable Zinc-air battery (Jing Zhang, et al., Front. Phys. 18(1), 13603 (2023)).

In this project we focused on the cathodic compartment of the RZAB, particularly, the cathodic compartment. The electrochemical reactions that take place in the cathodic compartment are the oxygen reduction reaction (ORR) during the discharging process and the oxygen evolution reaction (OER) during the charging process.In a typical RZAB, during the discharging of the cell, the oxygen reduction reaction takes place as shown in Equation 1, whilst in the charging process the oxygen evolution reaction takes place, as shown in Equation 4. In ORR, O_2 can directly be reduced into hydroxyl anions (OH^-) in alkaline media (Equation 1). This is the most favorable electrochemical reaction however, an electrocatalyst may reduce O_2 *via* a two-electron pathway in which O_2 is first reduced to hydrogen peroxide (HO_2^-) (Equation 2) and further reduced to hydroxyl ions (OH^-) as shown in Equation 3 below. [8,9]

ORR :Direct pathway $O_2 + 2H_2O + 4e^- \rightarrow 4OH^-$ (1)

Indirect pathway $O_2 + H_2O + 2e^- \rightarrow HO_2^- + OH^-$ (2)

$HO_2^- + H_2O + 2e^- \rightarrow 3OH^-$ (3)

OER : $4OH^- \rightarrow O_2 + 2H_2O + 4e^-$ (4)

The ORR and OER exhibit high overpotentials and sluggish reaction kinetics due to their inherent complexity. Therefore, the development of an effective cathodic catalyst is crucial for enhancing the efficiency of oxygen electrocatalyst and enabling its utilization in rechargeable metal-air batteries. Currently, state-of-the-art catalysts that are used in the cathodic compartment of the rechargeable zinc-air battery are made of expensive platinum (Pt)-based materials [10]. Consequently, significant research efforts have been dedicated to developing alternative catalysts that possess desirable traits of efficiency, stability, and cost-effectiveness. Exploration has been conducted on non-noble transition metal catalysts, including high-porosity carbons with or without the incorporation of transition metals. [10] In this research project, metallotetraporphyrazines shown in Figure 2, in which iron (Fe) and cobalt (Co) are the metal centers were explored as

electrocatalysts towards ORR and OER in alkaline electrolyte. They have four pyrrolic rings connected and held in place by aza nitrogen atoms, they are low cost, have stable, rich oxidation chemistry and have MN_4 moieties which are ORR and OER active catalytic sites, they also have double bond which make them good pi donors and good pi acceptors. [11,12] Mxenes (Ti_2CT_x), which are 2D nanomaterials are good electrocatalysts for applications in energy storage due to their unique structure, these 2D nanomaterials can be layered to sheets to enhance their electrochemical performance. [13,14,15] Mxenes are applied in many industries such as water purification, energy storage, biomedical and electrocatalysis. [13,14,15] The layered 2D sheets allow for metal ion intercalation, which results in Mxene with intercalant showing improved conductivity and other electrochemical properties. They are also less prone to corrosion unlike carbon, which is mostly used for electrocatalyst support. [13,14,15]

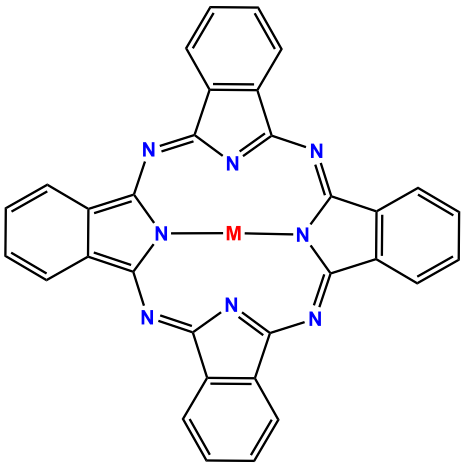

Figure 2: The structurer of metalloporphyrazine complex.

The Fe and Co central atoms of the catalyst complex can show favourable catalytic performance when intercalated in Mxenes for the ORR and OER processes in electrochemical devices via an approximated 4-electron transfer pathway and the positive onset potential by experimental method. [13,14,15] The natural abundance of the transition metal catalysts and the stability when supported on the Mxene sheets is proposed to be relatively good compared to platinum supported on carbon as an electrocatalyst, as it is prone to instability at high overpotentials since platinum may be oxidized to platinum oxide

and carbon can be easily corroded. [16] Therefore, in this work for the first time we present the use of a composite electrocatalytic material, consisting of Fe-tetraporphyrazine and Co-tetraporphyrazine intercalated in Mxene sheets (Scheme 1) with low carbon content as an electrocatalyst for ORR and OER in alkaline electrolyte.

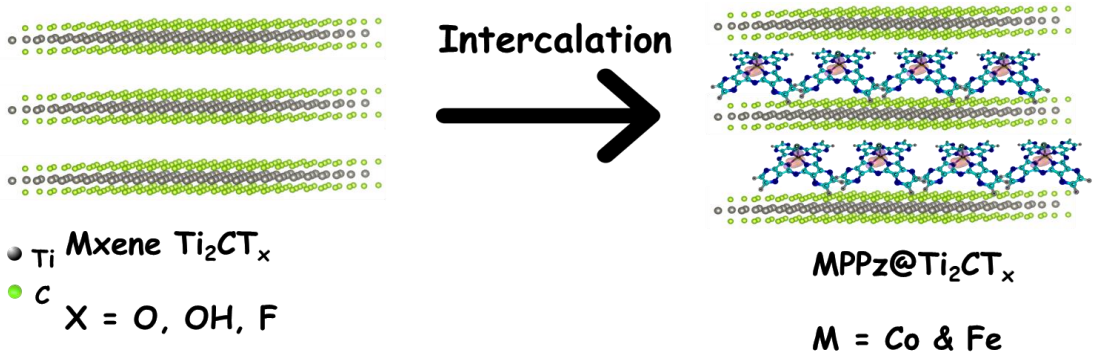

Scheme 1: Schematic diagram illustrating the intercalation of the complexes in MXene layered sheets.

Furthermore, the physical characterizations using Ultraviolet-Visible (UV-Vis.) spectroscopy, X-ray diffraction (XRD) and scanning electron microscopy (SEM) as well as electrochemical characterizations, such as cyclic voltammetry (CV), linear sweep voltammetry (LSV), and electrochemical impedance spectroscopy (EIS) were used to test and evaluate the properties of the electrocatalyst. To characterize the electrocatalysts' activity for towards ORR and OER was conducted using rotating disk electrode (RDE).

Experimental Procedure

Materials

Maxthal 211 (MAX) (Ti_2AlC powder >90 wt% purity; Kanthal AB, Sandvik Materials Technology, Sweden; <45 mm particle size). Ketjen black (KB). Iron Chloride ($FeCl_2$), cobalt chloride hexanitrate ($CoCl_2 \cdot 6H_2O$), lithium fluoride (LiF) and Nafion® were bought from Sigma Aldrich. The potassium hydroxide (KOH) pellets, hydrochloric acid (HCl), N,N-Dimethylformamide (DMF) were purchased form ACE chemicals. Ethanol (EtOH, 99%) was purchased from MK chemicals. Ultra-pure water of resistivity 18.2 Mcm^{-1} was

collected from a Milli-Q Water System. Oxygen gas was supplied by Afrox (South Africa).

Synthesis of Mxene (Ti_2CT_x)

MXene, Ti_2CTx, was synthesized by wet chemical exfoliation of the commercial Ti_2AlC, Maxthal® 211, powder following the in-situ HF procedure as shown in Scheme 2 below. An in-situ HF etching method was used because of safer conditions and less aggressive nature as compared to concentrated HF acid. The mild LiF+HCl (in situ HF) solution was prepared by dissolving 2 g of LiF salt into 40 mL of 6 M, HCl solution. After complete dissolotuion of the salt, 2 g of Ti_2AlC powders were gradually added to the in-situ HF solution. The gradual addition of the MAX bulk was necessitated by an exothermic nature of the exfoliation reaction. As soon as Ti_2AlC was completely immersed into the in-situ HF solution, the mixture was heated to 40 ^oC while stirring for 48 hours. Subsequently, after 48 hours, the mixture was centrifuged and washed with deionized water and rinsed with ethanol a couple of times until the supernatant reached a pH of approximately 6. Finally, after washing and rinsing, the obtained powder Mxene (Ti_2AlC) powder was dried in a vacuum oven for 48 hours at 45 ^oC.

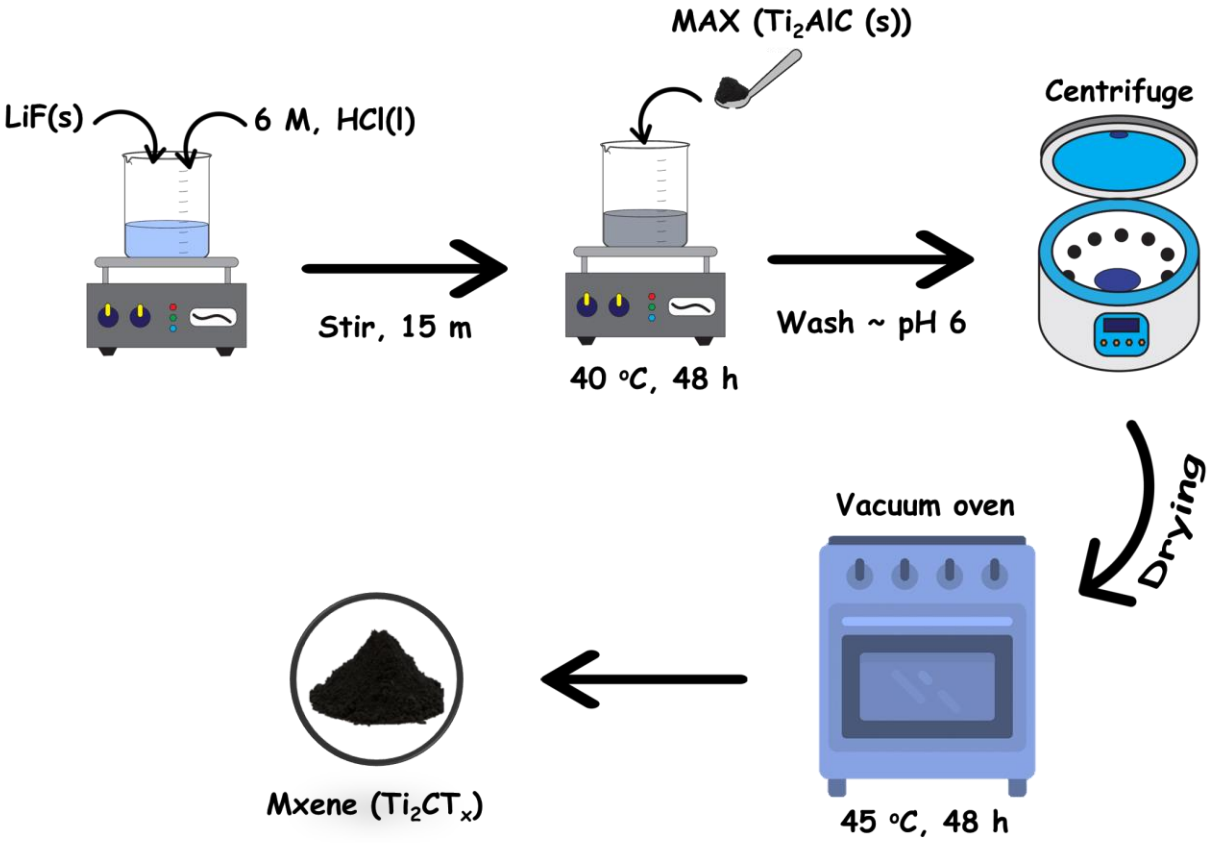

Scheme 2: Schematic diagram showing the synthesis of MXene.

Synthesis of Iron and Cobalt-tetraporphyrazine (FePPz) and (CoPPz)

Typically 1.0 mmol of $CoCl_2 \cdot 6H_2O$ and 4.0 mmol 2,3-pyrazinedicarbonitrile were fully dissolved in ethylene glycol by stirring for an hour. Then, the mixture was subjected to microwave irradiation at 600 W for 5 minutes, followed by washing with methanol and water, using a centrifuge (4500 rpm, 5 cycles each). The solid was dried in a vacuum oven for 24 hours at 60 ºC and the CoPPz was obtained and collected in a polytope vial. The same synthesis procedure was followed for FePPz. The schematic diagram showing the synthesis of the complexes are shown below (Scheme 3).

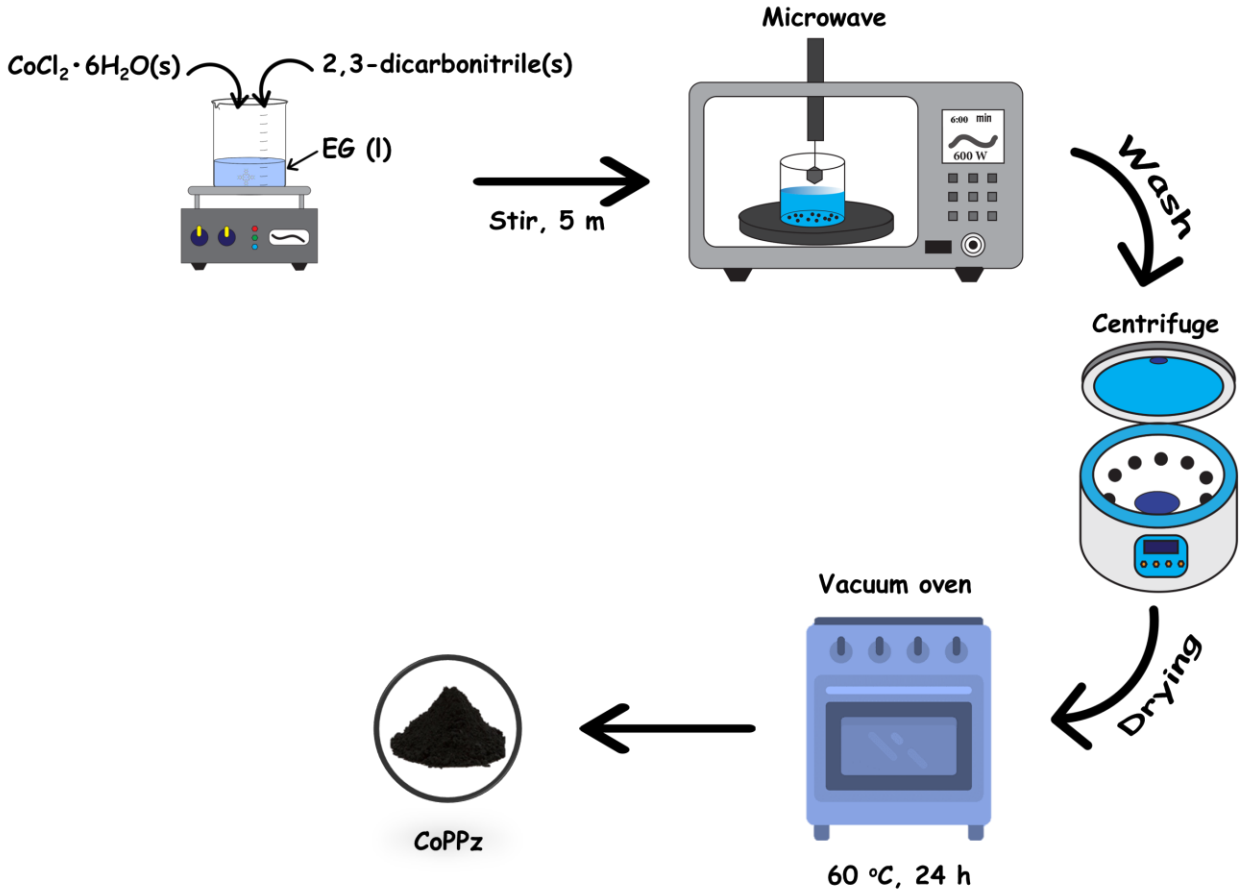

Scheme 3: Schematic diagram showing the synthesis of the CoPPz complex.

Synthesis of the composite FePPz/Ti_2CT_x and CoPPz/Ti_2CT_x

The schematic diagram shown in Scheme 4 shows the preparation of the composites. Ti_2CT_x (0,425 g) along with 15.0 % of CoPPz (0,075 g) intercalant, were weighed and added into vials respectively. Ti_2CT_x was delaminated by DMF (30mL) in a beaker while the CoPPz was dissolved in DMF 30mL in a round bottom flask. Both mixtures were sonicated at room temperature for 1 hour 30 minutes for them to be fully dispersed. The delaminated Ti_2CT_x in DMF solution was stirred at 1000 rpm with CoPPz intercalant being added slowly, dropwise, to the mixture. The mixture was then stirred for a further 48 hours in a fume booth with parafilm used to prevent the solvent from evaporating.

After stirring for 48 hours, the composite solution was centrifuged for separation. DMF was decanted and the solution was dried at a temperature of 60ºC in an oven for 24 hours to which the obtained material after drying for 24 hours was stored in a poly-top vial. The same synthesis procedure was followed for FePPz/Ti_2CTx.

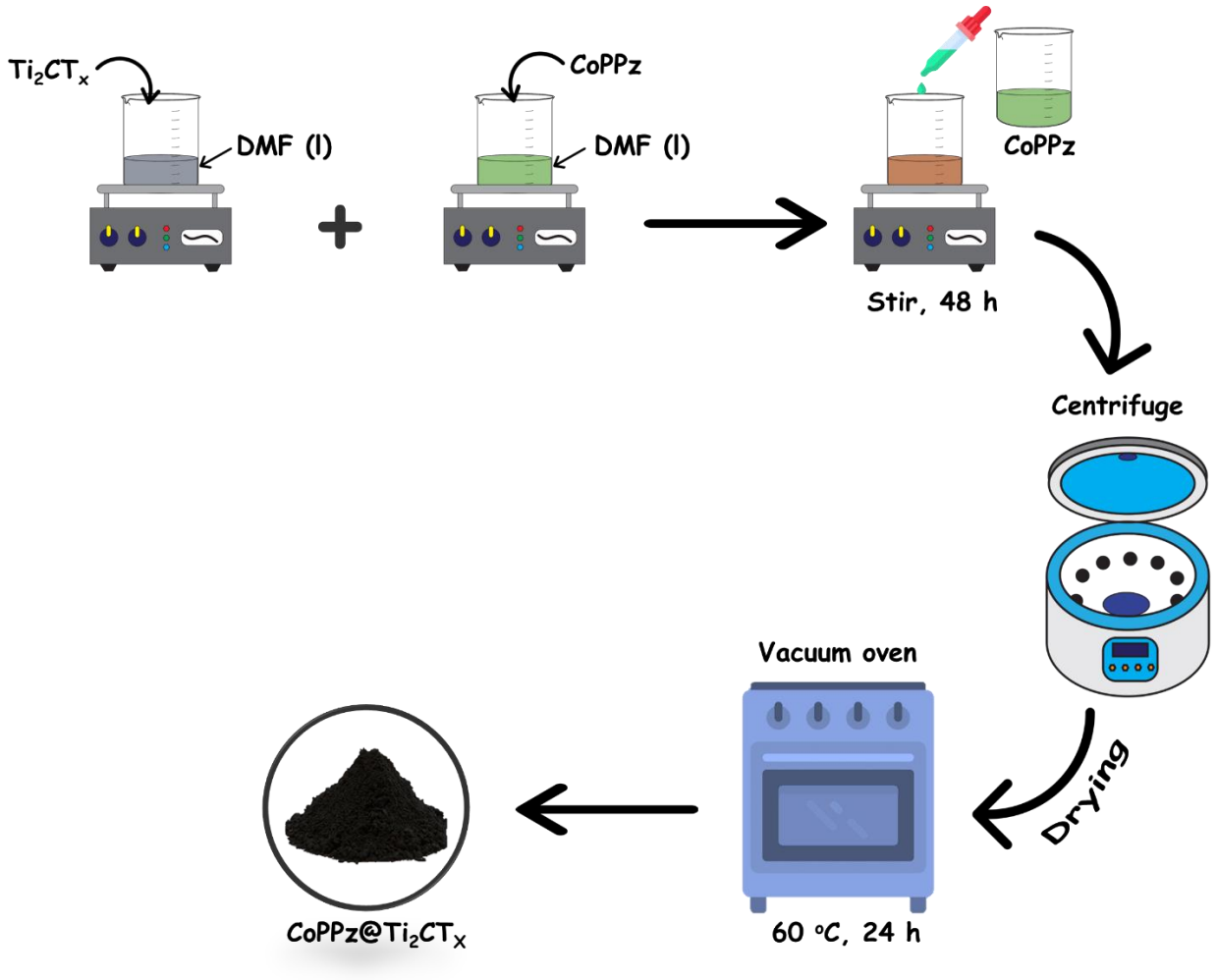

Scheme 4: Schematic diagram showing the synthesis of the CoPPz/MXene composite.

Ink preparation

The composite material, CoPPz/Ti_2CT_x (5.01mg) was weighed into a vial. The material was then dispersed in 500µL of a mixture consisting of ethanol (7.5 mL), water (2.5 mL)

and Nafion (0.5 mL) solvent through ultrasonication for 30.0 min, resulting in an ink solution.

Electrochemical measurements of $FePPzTi_2CTx/KB$ and $CoPPzTi_2CTx/KB$

Electrochemical measurements were conducted using a rotating disk electrode apparatus being directly controlled by the Biologic SP300 Potentiostat, driven by EC-lab 11.42 version software. All the electrochemical measurements were carried out at room temperature in a single compartment, three-electrode cell. A silver-silver chloride reference electrode (Ag/AgCl), a platinum wire (Pt) counter electrode and a glassy carbon (GC) RDE working electrode were all used. The techniques used in this research are cyclic voltammertry (CV) and electrochemical impedence spectroscopy (EIS) An aliquot of 30µL of the ink was drop casted onto the polished RDE glassy carbon electrode of 5,0mm diameter and allowed to dry at room temperature. Rotating disk electrode (RDE) measurements were performed in a 1.0 M KOH electrolyte which was prepared by dissolving KOH pellets (5.6102 g) in 100mL of ultra-pure water in a volumetric flask. The CV in O_2 saturated electrolyte was run at a scan rate of 50 mV/s in this potential window (-1.0 – 0.2 V vs Ag/AgCl). ORR was run at the 1600 rpm rotation rate under the same potential window, at a scan rate of 10mV/s. OER was run at 10mV/s at a potential window of (-1. 0 – 0.2 V vs Ag/AgCl) and using 1600rpm rotation rate. EIS was run at a the half-wave potential ($E_{1/2}$) and frequency range of 100kHz to 0,1 Hz at 1600rpm.

Results and Discussion

X-ray Diffraction

This technique was used to determine the crystal structure of Mxene, this is a non-destructive technique that shines X-ray beams to a sample to get characteristic diffractograms. The X-ray diffractions of precursor parent MAX phase (Ti_2AlC) and the synthesized pristine Mxene (Ti_2CT_x) are displayed in Figure 3. The diffractograms of the MAX phase confirms the composition by the pronounced characteristic peaks (002), (101), (102), (103), (106), (107) and (110). The as received Maxthal 211 powder before

etching consists mainly of Ti_2AlC (JCPDS 01-081-8106), with minor quantities of Ti_3AlC_2 (JCPDS 04-012-0632), TiC (JCPDS 01-089-3828) and Ti_xAl_y (JCPDS 04-007-2382, 01-074-4925, 04-007-2383 and 01-081-9785). These phases were also observed by other researchers who worked with the same material obtained from the same source (Journal of The Electrochemical Society, 165 (3) A501-A511 (2018)). After the exfoliation of Al through wet chemical etching using an acid, the synthesis of Mxene is successful, which is suggested by the (002) peak that moved to lower two theta angle values. This peak moving to low two theta angles implies that the interlayer spacing increases, indicating that the lattice parameter increases, which is characteristic of the conversion of MAX to Mxene nanosheets that have surface terminating groups, which are -O, -OH, -Cl and -F. The nanosheets are known to be negatively charged and hydrophilic, making Mxene to be able to absorb poor solvents which are useful in expanding the interlayer spacing.

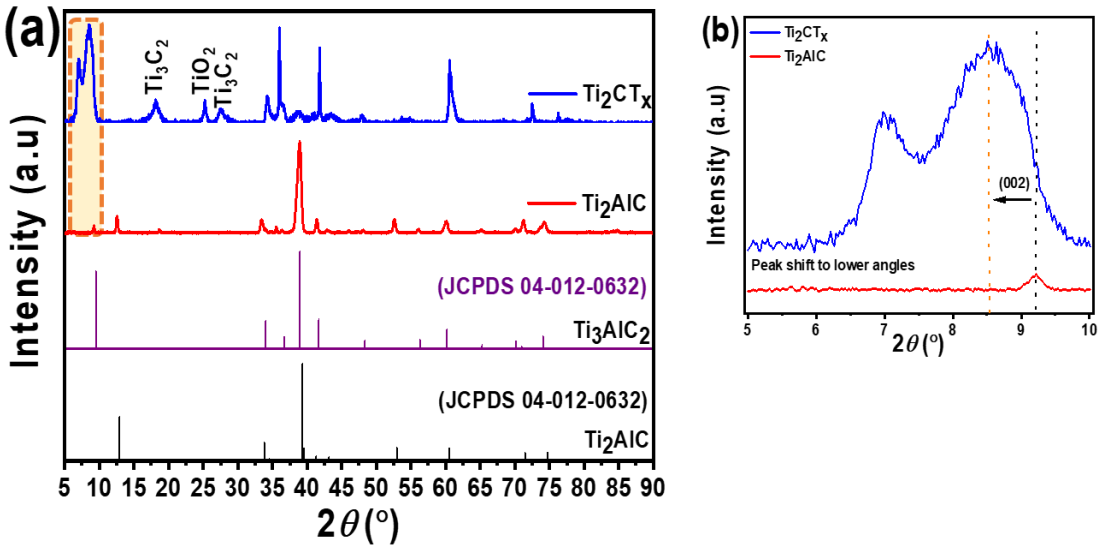

Figure 3: XRD diffractogram of (a) MAX and MXene (b) zoomed (002) peak.

Ultraviolet-Visible light spectroscopy (UV-Vis)

UV-Vis is an analytical technique that exposes ultraviolet/visible radiation to matter and based on the characteristic interaction of the matter with the radiation, a characteristic signal on the spectrum is created. Figure 4 shows the UV-Vis spectra of iron and cobalt

tetraphorphyrazine complexes. In Figure 4, the metallotetraporphyrazines exhibit two sets of bands, the B and Q bands, on the spectrum. The Q band is around 630nm for both complexes is observed and can be attributed to the pi – to – pi (π to π) interactions on the molecule. The B band is due to the MN4 back bone and the weak peak around 450 nm for both complexes are due to the metal to ligand interaction. The CoPPz material shows a very weak peak and not prominent compared to the FePPz. This could be due to lower fraction of the metal to ligand bonds compared to FePPz. It could also be due to the metal salt of cobalt being hydrated as opposed to that of iron which was anhydrous and could lead to poor complexation or the affinity for cobalt to nitrogen being very low compared to the affinity of iron to bond with nitrogen. [10]

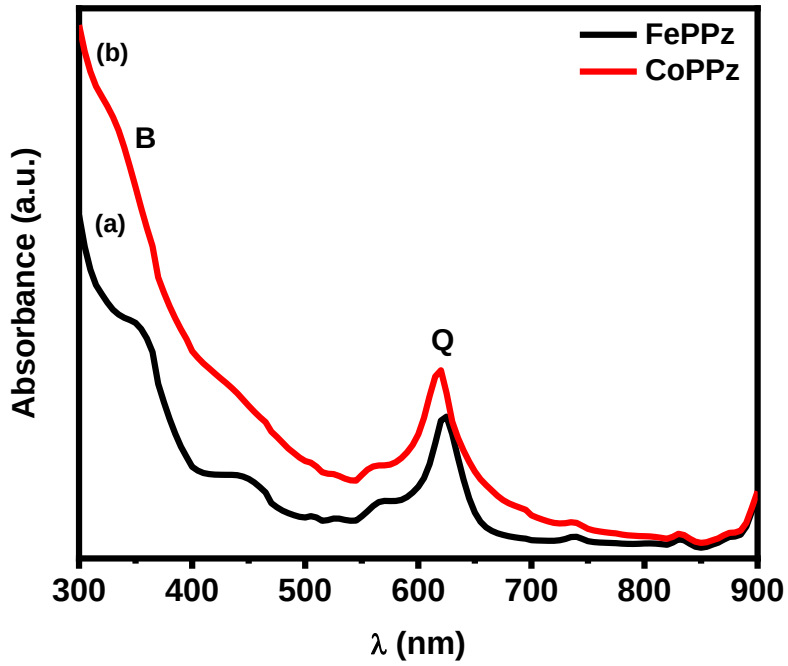

Figure 4: UV-Vis. spectrometry for the Fe and Co – tetraphorphyrazine complexes.

Scanning Electron Microscopy

This technique uses electrons to obtain the surface morphology of the material which works by directing electrons the electrons to the material where they are absorbed, reflected, and released as secondary electrons, after which the machine detects and processes the electrons to create an image of the material. As seen in Figure 5, the exfoliation of the closely packed MAX (Figure 5a) is indicated by the SEM images in Figure 5b showing that the obtained material is a 2D-layered structure. This supports the 002 peak shift in XRD and shows that the synthesis of Mxene was successful.

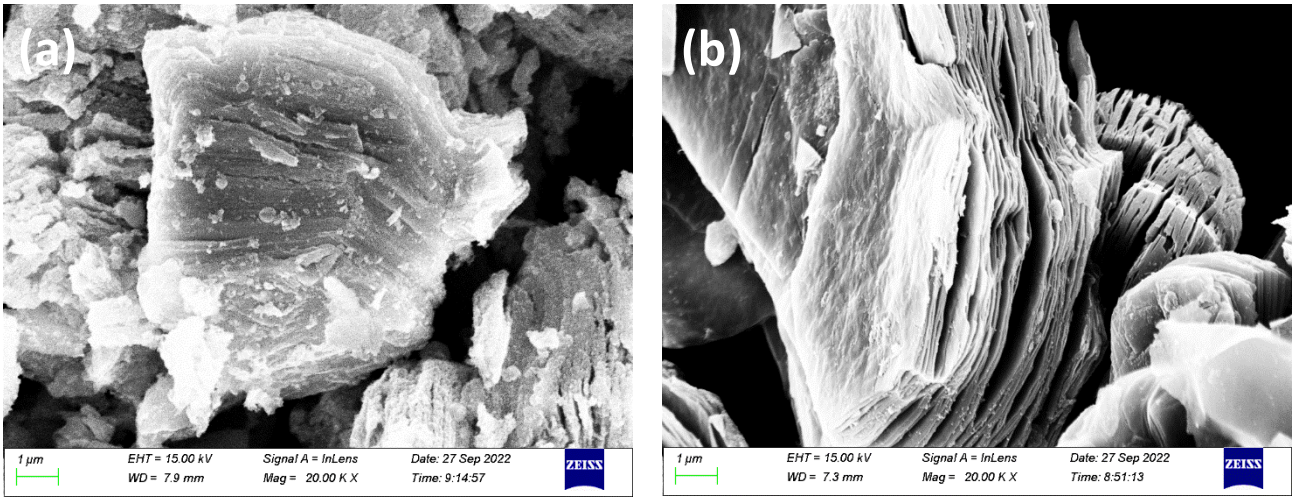

Figure 5: SEM images of the (a) MAX and the (b) MXene phase.

Electrochemical Characterization

The electrocatalytic performance of the materials FePPz/Mxene/KB and CoPPz/Mxene/KB was assessed in a three-electrode system containing a 1.0 M KOH electrolyte purged with O_2 gas. Figure 6 shows the CV and the LSV profiles of the KB, MXeneKB, FePPz/Mxene/KB and CoPPz/Mxene/KB. As seen from Figure 6 (a), the CV and Figure 6 (b) shows the activity of the electrocatalyst at 10 mV/s collected at 1600rpm. FePPz/Mxene/KB electrocatalyst performs better than the CoPPz/Mxene/KB electrocatalyst showing an earlier onset potential compared to that of the latter catalyst which is late. From the half wave potential values seen in Table 1, it can also be noted that FePPz/Mxene/KB has a larger value compared to the CoPPz/Mxene/KB, showing that the Fe catalyst shows better performance in the ORR process.

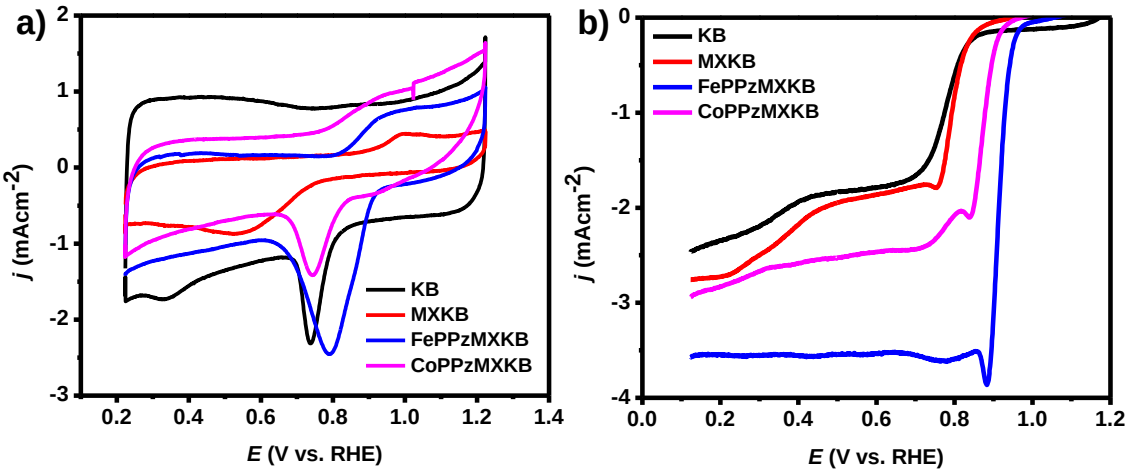

Figure 6: (a) The CV at 50 mV/s profiles and (b) LSV at 10 mV/s collected at 1600 rpm profiles of the materials in 1.0 M KOH saturated with O_2.

Figure 7 shows the Nyquist plots obtained from the EIS, this plot shows two arcs for each electrocatalyst being studied. The arc indicates the presence of the solution resistance and the charge transfer resistance, R_s and R_{CT} respectively. The R_s indicates the wettability of the electrocatalyst and R_{CT} indicates the measure of the electron transport. As seen in the plots, FePPzMxeneKB shows a smaller R_s, illustrating easier wettability of the electrocatalyst as well as a smaller R_{CT} value indicating faster electron transport compared to CoPPzMXeneKB. This can be because FePPzMexneKB formed better metal to ligand bonds, which indicates better complexation, this ultimately indicates better formed ORR catalytic sites leading to better catalytic performance for this ORR process. This can also be seen from the UV-Vis spectrum in figure 4, where FePPzMxeneKB has a prominent Metal to ligand interaction peak around 450 nm compared to CoPPzMxeneKB peak.

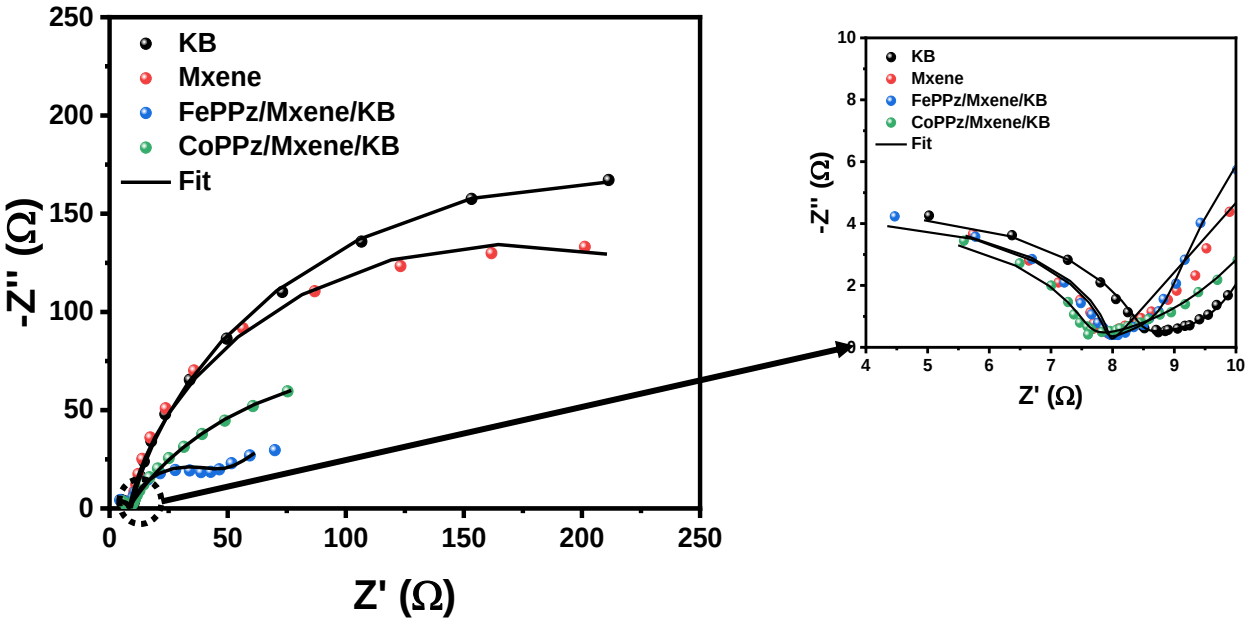

Figure 7: Nyquist plots of the electrocatalysts at the $E_{1/2}$ conducted in O_2 sat'd 1.0 M KOH

Furthermore, EIS was carried out to investigate the electrochemical properties of electrocatalyst in KOH electrolyte. The Nyquist plots were fitted to circuit components, such as the solution resistance (Rs), charge-transfer resistance (Rct), interfacial resistance (Rint), constant phase element (CPE) and electric double-layer capacitance (Cdl). At the low-frequency range, the Nyquist plots of KB, Mxene, FePPz/Mxene/KB and CoPPz/Mxene/KB showed the Rs values of 0.74, 0,29, 0,14 and 0.45, respectively. The high Rs value of CoPPz/Mxene/KB is attributed to the low conductivity as well as poor coordination between the metal and ligand as suggest in Figure 4b. In addition, at the high-frequency range, the smaller semicircle of the FePPz/Mxene/KB as compared to other electrocatalyst revealed lower charge transfer resistance as shown in Table 1 and the inset of Figure 7. Table 1 below summarizes all the EIS parameters for all electrocatalyst.

Table 1: EIS parameters for all electrocatalyst.

EIS parameters	Materials KB	Mxene	FePPz/Mxene/KB	CoPPz/Mxene/KB
R_s (Ω)	0.74 ± 0.04	0.29 ± 0.01	0.14 ± 0.01	0.45 ± 0.01
R_{ct} (Ω)	8.28 ± 0.83	7.52 ± 0.03	7.79 ± 0.44	7.14 ± 0.14
R_{int} (Ω)	378 ± 37.8	203. ± 42.63	22.73 ± 1.63	238 ± 108.3
R_{SEI} (Ω)	1.63 ± 0.08	0.52 ± 0.01	-	1.49 ± 0.81
C_{dl} (µF)	0.16 ± 0.04	3.72 ± 0.25	3.62 ± 0.45	0.22 ± 0.01
***CPE_{ct}* (mF. s^(a-1))**	3.63 ± 0.06	0.03 ± 0.01	18.20 ± 0.23	11.52 ± 0.02
a	0.90	0.57	0.1	0.68
***CPE_{ct}* (mF. s^(a-1))**	4.92 ± 0.09	0.21 ± 0.03	33.67 ± 7.59	10.99 ± 6.68
a	0.60	0.87	0.55	0.70

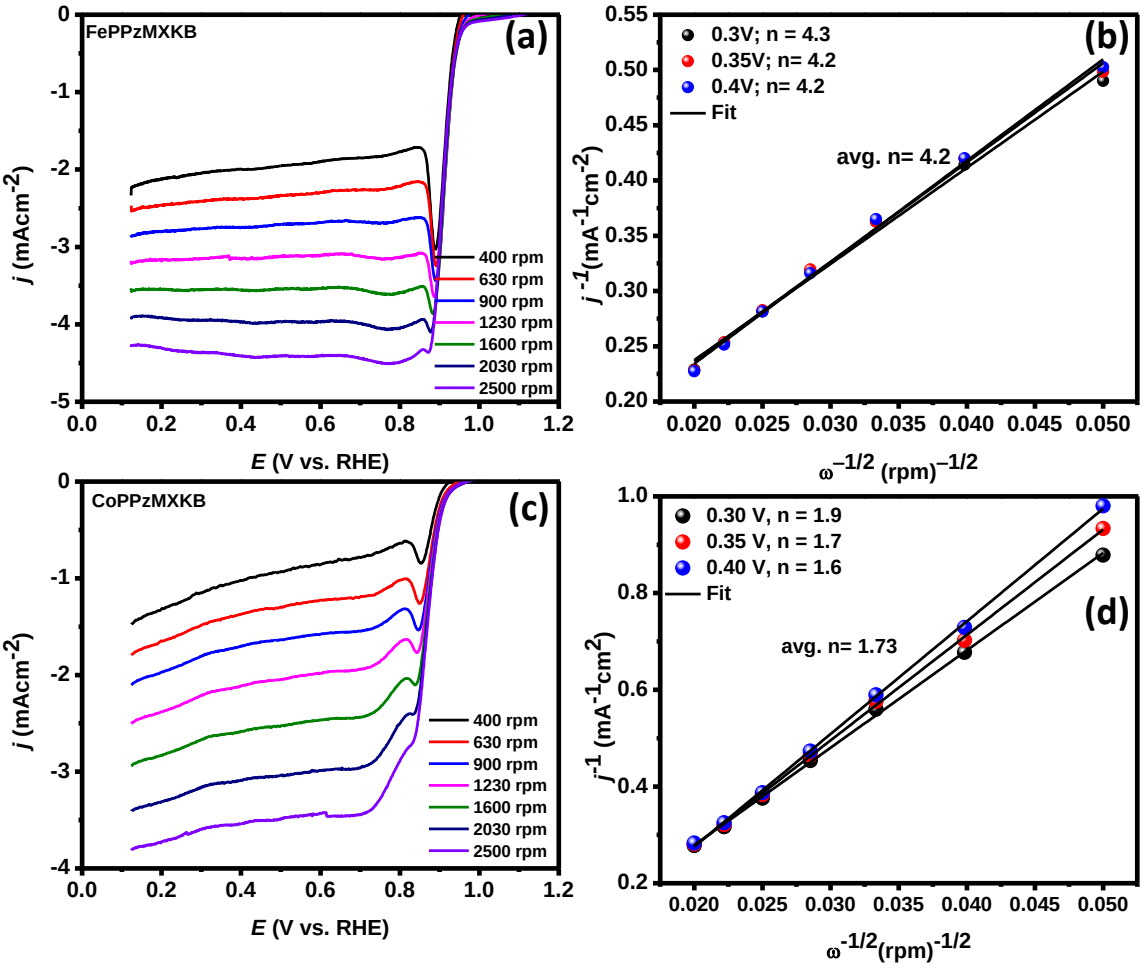

Figure 8: (a,c) LSVs profiles of the FePPzMXeneKB and CoPPzMXeneKB at various rotations and the corresponding Koutecky-Levich plots.

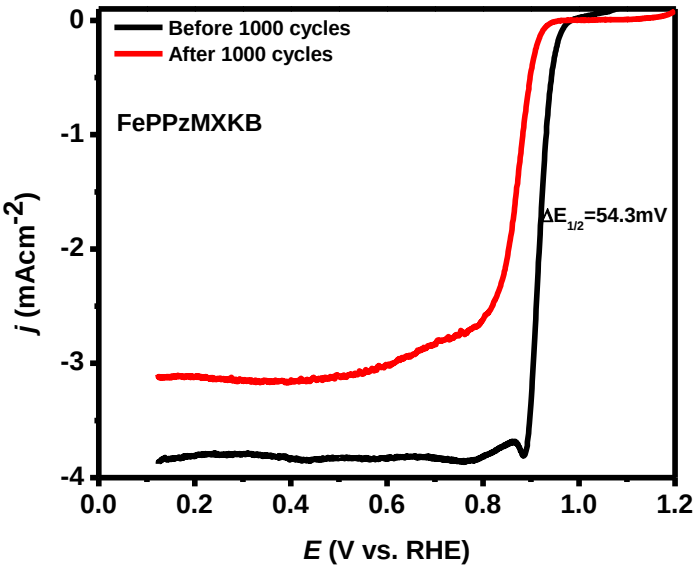

Figure 9: LSVs of the FePPzMX/KB before and after 1000 cycles.

Figure 9 shows the voltammogram for the OER electrochemical characterization. The Co catalyst shows better performance when compared to the Fe catalyst because at the potential (E) where the current density is 10 mA cm^{-2}, the potential for CoPPzMxeneKB is lower than FePPzMxeneKB and this is a merit used to measure the catalytic activity for the OER process. Table 1 summarizes the information obtained from the ORR and OER polarization curves and it should be noted that FePPzMxeneKB showed favorable catalytic activity for ORR and CoPPzMxeneKB showed favorable catalytic activity for OER. In addition, the delta E value which is calculated by taking the difference between $E_{1/2}$ (ORR) and $E_{@\ 10\ mA\ cm^{-2}}$ (OER) was determined. This parameter is used to calculate the bifunctionality which is an indicator used to characterize electrocatalysts for the rechargeable zinc-air batteries. It measures the potential gap required to reverse from OER to ORR during the charging and discharging process cycles. A smaller value is ideal indicating the lower energy barrier required for reversibility. In this study, FePPzMxeneKB yielded a lower delta E value, showing an appreciable low value, showing promising results.

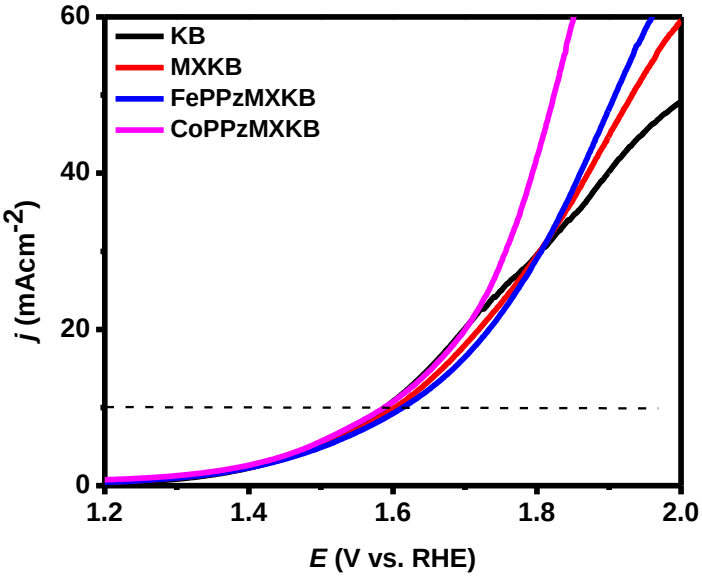

Figure 10: LSV of the electrocatalysts for OER.

Table 1: ORR and OER parameters summary

Electrocatalyst	$E_{1/2}$ (V)	E @ 10 $mAcm^{-2}$ (V)	$\Delta E = E_{1/2}$ - E @ 10 (V)
KB	0.774	1.58	0.798
MXKB	0.802	1.58	0.778
FePPzMXKB	0.926	1.60	0.674
CoPPzMXKB	0.879	1.62	0.741

Conclusion

The ORR and OER results indicate that both the electrocatalysts showed good electrocatalytic activity for the ORR and OER processes in 1.0M KOH. From the EIS data, a smaller charge transfer resistance was observed for FePPzMXene/KB indicated by a smaller arc compared to the CoPPzMXene/KB electrocatalyst for ORR in 1.0M KOH. Also, an easier wettability of the FePPzMXene/KB electrocatalyst was indicated by the smaller R_s value. This is also good for a catalyst during the electrochemical reactions since it will minimize resistance for good electron transport. For the OER plot, the CoPPzMXene/KB catalyst showed an E value at 10 (mA cm^{-2}) that was lower than that of FePPzMXene/KB catalyst, meaning that the Co catalyst showed good performance for the OER process. Most importantly it was noted that, the delta E value for the Fe catalyst was lower, due to the more positive $E_{1/2}$ which meant that ultimately, the Fe catalyst shows promising results as a potential bifunctional ORR and OER electrocatalyst that would be suitable for the rechargeable zinc-air battery. Therefore, we successfully prepared a bifunctional electrocatalyst, FePPzMXene/KB in this project and demonstrated its electrocatalytic properties for ORR and OER.

Future work.

Further characterizations on the composite material are needed, to confirm that the intercalation of the metallotetraporphyrazine in MXene sheets was successful. Also. characterizations including, BET for surface area evaluations of the catalyst, XPS to investigate the chemical states and the interactions between the complex and MXene.

References

(1) Gielena, D., Boshella, F., Saygin,D., Bazilian, M.D., Wagnera, N., and Gorini, R. 'The role of renewable energy in the global energy transformation', Energy Strategy Reviewsm, **2019**, 38–50.

(2) Perera, F.; Nadeau, K. Climate Change, Fossil-Fuel Pollution, and Children's Health. *New England Journal of Medicine,* **2022**, *386* (24), 2303–2314.

(3) *Diehl, A, Why is Energy Storage Such an Important Part of the Renewables Mix,* **2015**.

(4) Logeshwaran, N.; Ramakrishnan, S.; Chandrasekaran, S. S.; Vinothkannan, M.; Kim, A. R.; Sengodan, S.; Velusamy, D. B.; Varadhan, P.; He, J.-H.; Yoo, D. J. An Efficient and Durable Trifunctional Electrocatalyst for Zinc–Air Batteries Driven Overall Water Splitting. *Applied Catalysis B: Environmental,* **2021**, *297*, 120405.

(5) Song, K.; Wei, J.; Dong, W.; Zou, Z.; Wang, J. Fe3O4/N-CNTs Derived from Hypercrosslinked Carbon Nanotube as Efficient Catalyst for ORR in Both Acid and Alkaline Electrolytes. *International Journal of Hydrogen Energy,* **2022**, *47* (47), 20529–20539.

(6) Jin, Z.; Lyu, J.; Hu, K.; Chen, Z.; Xie, G.; Liu, X.; Lin, X.; Qiu, H.-J. Eight-Component Nanoporous High-Entropy Oxides with Low Ru Contents as High-Performance Bifunctional Catalysts in Zn-Air Batteries. **2022**, *18* (12), 2107207–2107207.

(7) Ren, R.; Liu, G.; Kim, J.-E.; Ryanda Enggar Anugrah Ardhi; Minh Tâm Tran; Mirabbos Hojamberdiev; Joong Hee Lee. Photoactive G-C3N4/CuZIF-67 Bifunctional Electrocatalyst with Staggered P-n Heterojunction for Rechargeable Zn-Air Batteries. **2022**, *306*, 121096–121096.

(8) Riyaz, M.; Gupta, S.; Goel, N. First Principle Studies to Tailor Graphene through Synergistic Effect as a Highly Efficient Electrocatalyst for Oxygen Evolution Reaction. *ChemPhysChem* **2021**, *22* (11), 1141–1147.

(9) Liao, X.; Lu, R.; Xia, L.; Liu, Q.; Wang, H.; Zhao, K.; Wang, Z.; Zhao, Y. Density Functional Theory for Electrocatalysis. *ENERGY & ENVIRONMENTAL MATERIALS* **2021**, *5* (1), 157–185.

(10) Fashedemi, O. O.; Ozoemena, K. I. Oxygen Reduction Reaction at MWCNT-Modified Nanoscale Iron(II) Tetrasulfophthalocyanine: Remarkable Performance over Platinum and Tolerance toward Methanol in Alkaline Medium. **2015**, *5* (29), 22869–22878.

(11) Fan, M.; Liu, P.; Cheng, Y.; Tang, H.; Jin, B.; Fang, P. Fe-N4/Co-N4 Active Sites Engineered Porous Carbon with Encapsulated FeCo Alloy as an Efficient Bifunctional Catalyst for Rechargeable Zinc-Air Battery. **2023**, *935*, 168107–168107.

(12) Kumar, A.; Yasin, G.; Tabish, M.; Das, D. K.; Saira Ajmal; Kumar, A.; Zhang, G.; Thandavarayan Maiyalagan; Saad, A.; Gupta, R. K.; Makhlouf, M. M.; Ibraheem, S. A Catalyst-Free Preparation of Conjugated Poly Iron-Phthalocyanine and Its Superior Oxygen Reduction Reaction Activity. **2022**, *445*, 136784–136784.

(13) Hong Ng, V.M.,Huang, H., Zhou, K., Lee, P.L., Que, W., Xu J.Z., and Kong, L.B. 'Recent progress in layered transition metal carbides and/or nitrides (MXenes) and their composites: synthesis and applications', Journal of Materials Chemistry A, 5(7), **2017**, pp. 3039–3068.

(14) Anasori, B., Lukatskaya, M. R. and Gogotsi, Y. '2D metal carbides and nitrides (MXenes) for energy storage', Nature Review Materials, 2(2), **2018**, pp 1-17.

(15) Alhabeb, M., Maleski,K., Anasori, B., Lelyukh, P., Clark, L., Sin, S., and Gogotsi, Y. 'Guidelines for Synthesis and Processing of Two-Dimensional Titanium Carbide (Ti3C2Tx MXene)', Chemistry of Materials, 29(18), **2017**,pp. 7633– 7644.

(16) Habib, I.; Friedrich, A.; Ray, S. C.; Ozoemena, K. I. Interrogating the Impact of Onion-like Carbons on the Supercapacitive Properties of MXene (Ti_2CT_X). **2019**, *126* (13), 134301–134301.

R_Pheletso M_ Hons Research Project 1st draft.docx

ORIGINALITY REPORT

15%	11%	9%	2%
SIMILARITY INDEX	INTERNET SOURCES	PUBLICATIONS	STUDENT PAPERS

PRIMARY SOURCES

1	Submitted to Universiteit van Amsterdam Student Paper	1%
2	worldwidescience.org Internet Source	1%
3	Submitted to University College London Student Paper	1%
4	epdf.pub Internet Source	1%